Journal Pre-proofs

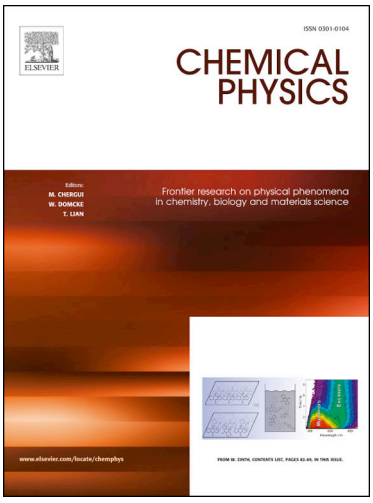

Tunable electro-optical properties of doped chiral graphene nanoribbons

Hazem Abdelsalam, Vasil A. Saroka, Mohamed M. Atta, Waleed O. Younis, Qinfang Zhang

PII: S0301-0104(21)00027-6
DOI: https://doi.org/10.1016/j.chemphys.2021.111116
Reference: CHEMPH 111116

To appear in: *Chemical Physics*

Received Date: 20 July 2020
Revised Date: 3 October 2020
Accepted Date: 12 January 2021

Please cite this article as: H. Abdelsalam, V.A. Saroka, M.M. Atta, W.O. Younis, Q. Zhang, Tunable electro-optical properties of doped chiral graphene nanoribbons, *Chemical Physics* (2021), doi: https://doi.org/10.1016/j.chemphys.2021.111116

Tunable electro-optical properties of doped chiral graphene nanoribbons

Hazem Abdelsalam[1,2], Vasil A. Saroka[3,4], Mohamed M. Atta[5], Waleed O. Younis[6], Qinfang Zhang[1*]

[1]School of Materials Science and Engineering, Yancheng Institute of Technology, Yancheng 224051, P. R. China. E-mail: qfangzhang@gmail.com

[2]Theoretical Physics Department, National Research Centre, El-Buhouth Str., Dokki,Giza, 12622, Egypt

[3]Institute for Nuclear Problems, Belarusian State University, Bobruiskaya 11, 220030 Minsk, Belarus

[4]Center for Quantum Spintronics, Department of Physics, Norwegian University of Science and Technology, NO-7491 Trondheim, Norway

[5]Radiation Physics Department, National Center for Radiation Researches and Technology (NCRRT), Atomic Energy Authority, Cairo, Egypt.

[6]Vice Presidency for Postgraduate Studies and Scientific Research, Imam Abdulrahman Bin Faisal University, P.O. Box 1982, Dammam, 31441, Saudi Arabia.

Abstract

The electro-optical properties of doped chiral graphene nanoribbons are investigated using first principles calculations. O-atoms on edges enhance edge reconstruction with strong C=C bonds that increase the binding energy while at the surface they break some surface bonds and decreases the binding energy. The energy gap in the former increases to 2.08 eV due to the passivation of edge electrons, while in the latter it becomes 0.07 eV. Electric field provides additional manipulation, for instance Y-field produces oscillation/decrease of the electronic and optical energy gap between the edge/surface states in undoped/O-B-O doped chiral nanoribbons.

Introduction

Graphene nanoribbons (GNRs) are flat sp2-carbon systems with widely tunable electronic, magnetic and optical properties [1–4]. The two simplest classes of GNRs have zigzag (Z) and armchair (A) edges. However, many more edge types are possible. Atomically tunable GNR structure makes them promising for electronic, optical and spintronic devices [5]. In recent years we have witnessed a formidable advance in synthesis of GNRs with controlled structural parameters: width, length and edge type [6]. The major method for gaining control over the GNR structure is the bottom-up self-assembling of molecular precursors which exists in forms of surface assisted [7] and solution based techniques [8,9]. A great variety of ribbons has been produced with the self-assembling such as armchair (including their lateral fusion [10–14]), zigzag [15], chiral [16], chevron [7,9], and some other ribbons that can be classified [17–19] as A60 (extended chevron) [20–22], A120 [23], Z60(cove-edged) [24] and Z120(zeeZGNR2) [25]. In on-surface molecular self-assembling the geometry of GNR is specified by the molecular precursor and the type of the metallic substrate [29,30]. One of the challenges is to produce GNRs characterized by zigzag edges and chirality being described by a large difference of crystallographic indexes n and m in the translation vector $\boldsymbol{C}_h = (n,m) = n\boldsymbol{a}_1 + m\boldsymbol{a}_2$, where $\boldsymbol{a}_{1,2}$ are graphene lattice primitive translations. Only two specie of chiral ribbons with translation vectors (3,1) [26] and (4,1) [27] have been obtained so far. Such ribbons have been produced

only by on-surface synthesis with Au(111) or (322) [28], Cu(111) and Ag(111) substrates. The structure an electronic properties of chiral ribbons have been studied with low-temperature scanning tunneling microscopy (STM) [16,26–29], non-contact atomic force microscopy(AFM) [30], Raman spectroscopy [27], scanning tunneling spectroscopy(STS) [28] and the angle resolved photoemission spectroscopy(ARPES) [28]. The conductive metallic substrate used in on-surface synthesis is readily suitable for STM studies of the electronic properties of these ribbons. The investigation of their optical properties, however, requires transferring them to an isolated substrate. For the atomically precise GNRs this has been demonstrated only for non-chiral GNRs of chevron-type obtained with solution based technique [9,20]. Thus, the optical properties of chiral ribbons remain elusive.

An insight into the optical absorption of very long GNRs can be achieved by linear mapping of experimental data of carbon nanotubes(CNTs) [31–34]. However, this mapping does not apply to the chiral GNRs and CNTs. The optical properties of quasi-infinite structures chiral GNRs have been considered in few studies where GNRs are treated within periodic framework [35,36]. At the same time, experimental structures are finite length ones with the majority of ribbon lengths <10-20 nm [29]. Finite length is a crucial factor for GNR integration into functional devices. Moreover, it has been shown by Raman spectroscopy performed on armchair GNRs that finite length effects are observable [37]. Preliminary theoretical studies of finite length (3,1) chiral GNRs have shown that the length of convergence of the electronic band gap to its bulk value (~5 nm) is shorter than that of the optical band gap (~25 nm) [38], thereby making optical properties more sensitive to the GNR length. Hence, a detail understanding is desirable with respect to the optical properties of finite length chiral GNRs.

Here, we investigate optical properties of (4,1) chiral GNRs. In addition to the width of the structures, we take into account their finite lengths. Since the self-assembling method allows for a precise positioning of the doping impurities [27,39], we also investigate the ways of effective electronic and optical engineering by substitutional doping. In case of transferring to the device substrate local electric fields may arise due to the impurities and imperfections of the substrate. Therefore, we supplement our study with the modeling of the effect of an external electric field. Within first principle density functional theory (DFT) calculations, we show that the considered systems can have wide range of physical properties starting from perfect edge conductors for topological insulators to wide band gap materials for photocatalytic applications. Additionally, these results must be useful in interpretation of experimental data and developing a reliable database for fast structural testing based on optical absorption spectroscopy methods similar to those being used for CNTs [40,41].

2. Computational model

In this work, we use the density functional theory in the investigations of the electronic and optical properties of chiral GNR. The calculations are performed using Gaussian 16 software [42] at the b3lyb/3-21g level of theory [43-46]. This level of calculations has been proved adequate with respect to both results accuracy and computational time for C-based materials [47-48]. For generalizing our work, we perform additional DFT calculations using VASP software for selected periodic chiral GNR. All VASP calculations were performed using the projector

augmented wave method (PAW) with a plane-wave basis set [49-52]. The Perdew-Burke-Ernzerhof (PBE) functional was used to describe the exchange correlation potential within the generalized gradient approximation (GGA) formalism [53]. The plane wave cut-off energy was set to 500 eV. The optimization of the bond lengths continues until the force on each atom becomes smaller in magnitude that 0.001 eV/ Å.

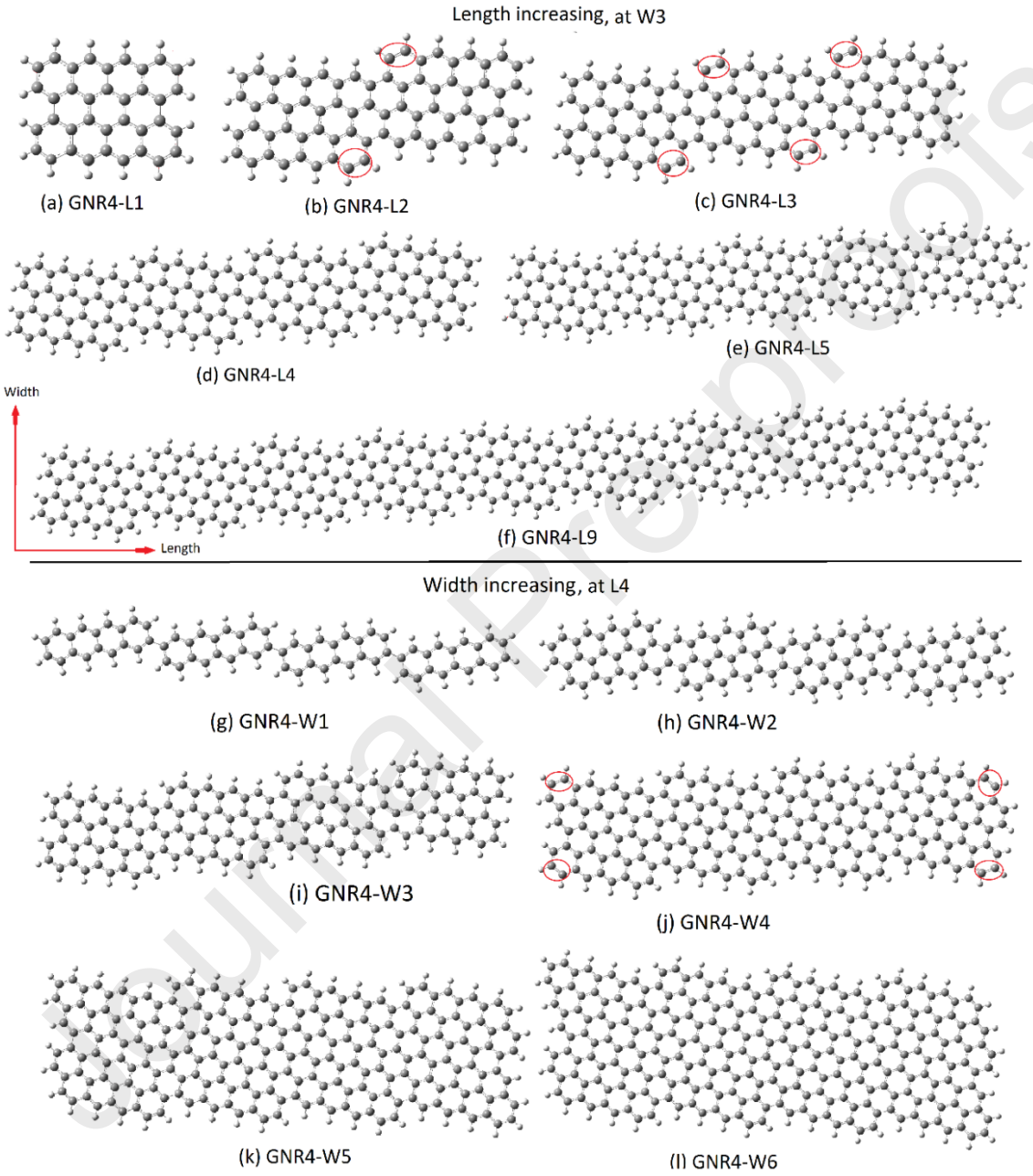

Fig. 1. Relaxed structures of chiral GNR4 with different lengths (a-f) and widths (g-l). The red circles shows the formed C=C bonds due to chirality.

3. Results and discussion

In order to simply express the chiral nanoribbons as a function of length and width, we use the form GNR4-W-L-X where 4 is the n index defining the translation vector, W, L, and X are the width, the length, and the dopant, respectively. When fixing width and varying length and vice versa (as shown in Fig. 1) we use only the variable parameter for instance GNR4-L1 in Fig. 1 (a) for fixed width W3.

3.1 Structure stability and electronic properties

The optimized structures of the finite chiral graphene nanoribbons with different lengths and widths are shown in Fig. 1. In addition to the optimized structures that are obtained by minimizing the total energy of the considered structure, the stability is also tested by calculating the vibrational frequencies and the binding energy. The obtained positive frequencies, see Fig. S_1 in supplementary material, indicate that the selected nanoribbons are geometrically stable and there are no saddle points on the potential energy surface. The following formula is used to calculate the binding energy per unit atom (E_B): $E_b= (N_HE_H+N_XE_X+N_CE_C-E_{Co})/N$. With, N_H, N_X, N_C, and N is the number of hydrogen atoms, doping X-atoms, carbon atoms, and the total number of atoms, respectively. E_H, E_X, E_C, and E_{Co} is the corresponding total energy, respectively. The binding energy used for testing stability, where the positive values of E_b insure the stability of the considered systems, can also be used to study the effect of size and doping on the binding strength. The binding energy calculations are given in Table 1. It is observed that E_b increases by increasing length and width simply due to the increased number of C-atoms that form three sigma bonds with adjacent C- atoms.

Table 1. Binding energy (E_B), energy gap (E_g), and total electric dipole moment (TEDM) of chiral GNR subjected to the effect of width/length and substitutional doping at the edge (e) and surface (s).

GNR4		**E_B (eV)**	**E_g (eV)**	**Doped GNR4-W3-L4**	**E_B (eV)**	**E_g (eV)**	**TEDM (D)**
Fixed width, W3	GNR4-L1	7.00	1.16	N-e	7.56	0.59	4.04
	GNR4-L2	7.28	0.75	N-s	7.34	0.53	12.64
	GNR4-L3	7.38	0.65	B-e	7.41	0.49	3.50
	GNR4-L4	7.43	0.61	B-s	7.29	0.44	12.18
	GNR4-L5	7.46	0.59	O-e	7.55	2.08	7.14
	GNR4-L6	7.49	0.57	O-s	7.17	0.07	28.01
	GNR4-L7	7.50	0.56	OBO-e	6.79	2.66	0.0001
	GNR4-L8	7.51	0.55	Cl-e	7.09	0.09	24.59
	GNR4-L9	7.52	0.54	Cl-s	7.55	0.20	4.27
Fixed length, L4	GNR4-W1	6.61	2.37	P-e	7.99	0.55	4.15
	GNR4-W2	7.06	0.22	P-s	7.08	0.76	9.94
	GNR4-W3	7.43	0.61	2P-e	7.36	0.54	0.0001
	GNR4-W4	7.67	0.52	S-e	7.27	1.85	1.62
	GNR4-W5	7.83	0.33	S-s	7.73	0.29	28.18
	GNR4-W6	7.95	0.17				

The effect of width on the binding strength is more significant than the effect of length because the number of edge atoms that bound to only two C-atoms in the later is higher than the former. For instance, for two ribbons with almost the same number of atoms but forming GNR4-W4-L4 (Fig. 1 (l), N=232 atoms) and GNR-W3-L5 (Fig. 1 e, 236 atoms), E_b= 7.7 eV in the former is higher than E_b= 7.4 eV in the later.

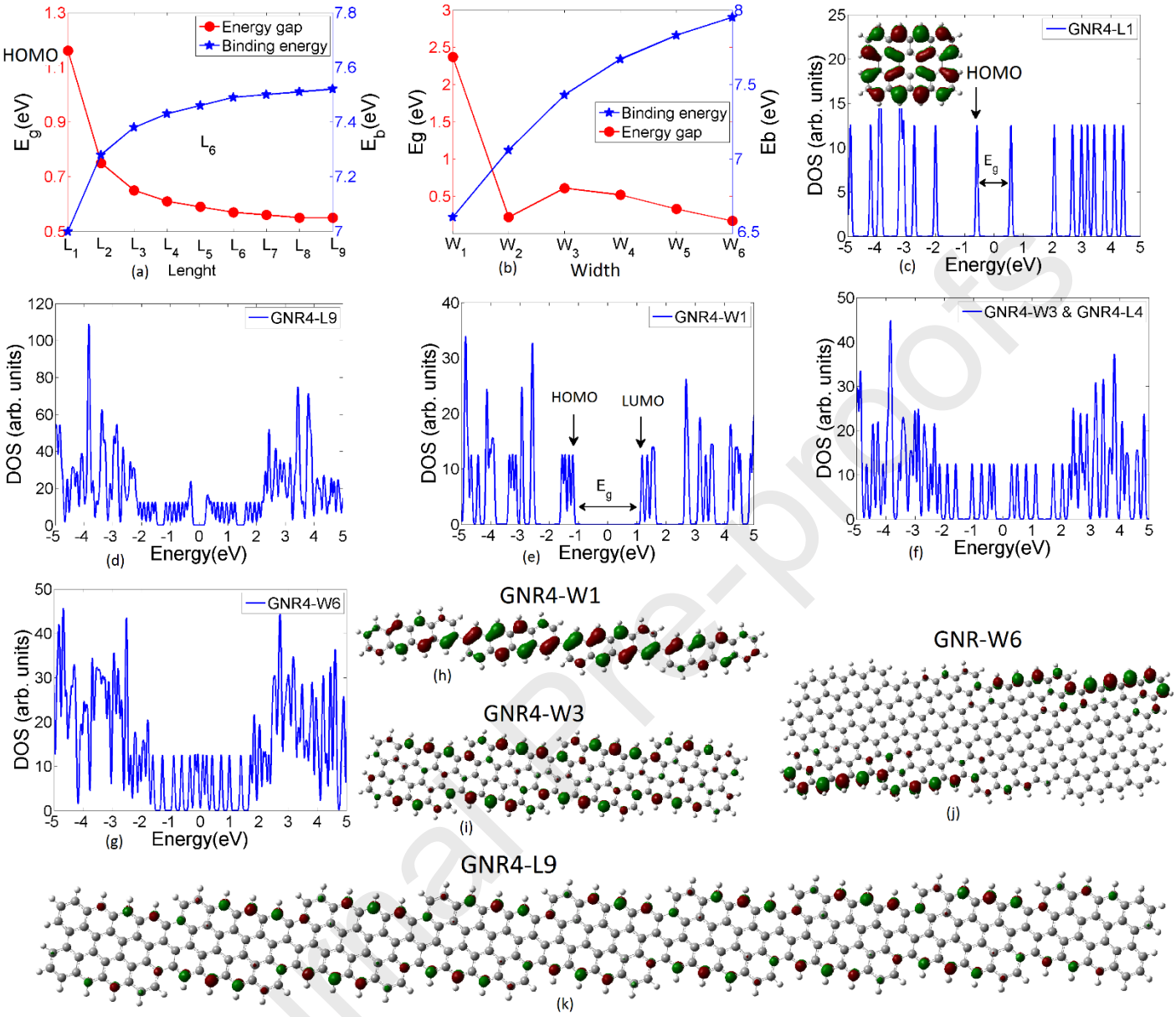

Fig. 2. The binding energy (E_b) and energy gap (E_g) dependence on the GNR4 length and width (a, b), the electronic density of states (DOS in c-g) and HOMO (h-k) for selected nanoribbons are presented.

The c-c bond lengths range from 1.36 to1.45 Å, the smaller values observed on the edges while the higher ones observed in the interior of the GNRs. Simultaneously with the increase of the binding energy the band gap decreases by increasing the GNR width and/or length. This decrease is a result of the quantum size effect and the previously described edge morphology. The energy gap smoothly decreases as a function of the length while as a function of width it decreases faster, similar to the jag parameters of zigzag-shaped ribbons in Refs [17-19]. Increasing the length by one unit-cell from GNR4-W3-L4 to GNR4-W3-L5 decreases the band gap from 0.61 to 0.59 eV, while increasing the width of the same ribbon to GNR4-W4-L4, E_g becomes 0.52 eV.

The origin of that effect is the type of bonds at the edges, where some C-atoms at the edges form double bonds with smaller bond length ~1.36 Å, see encircled bonds in Fig. 1 a, these bonds form molecular orbitals with energies deeper in the valance band than other edge bonds. The number of these energetically stable edge orbitals is higher in GNR4-W3-L5 than in GNR4-W4-L4. The type of the electronic states filling the band gap is the edges localized states as shown by the HOMO distribution in Fig. 2 (i-k). The antibonding nature of these pi-orbitals make them more interactive than the extended bonding pi-orbitals in Fig. 2 (c) and Fig. 1 (h). These edge states that provide perfect conduction at the edges and insulation at the surface of GNR4-W6-L4 (Fig. 2 j) indicate that such systems are promising materials in the field of topological insulators and should be considered by experimentalists working on this field.

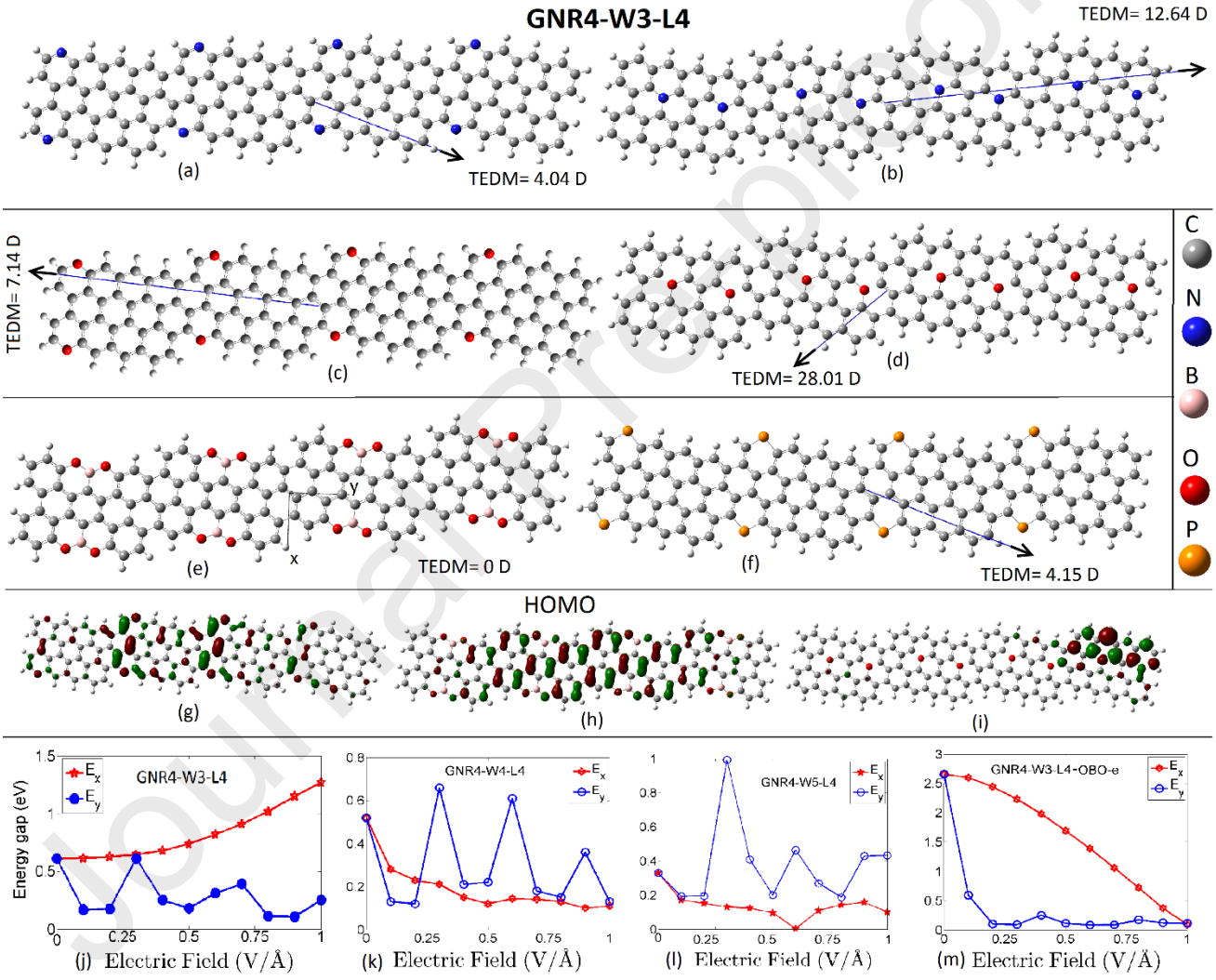

Fig. 3. Doped GNR4-W3-L4 with different atoms on the edge and surface (a-f), and the HOMO for O-, OBO- doped nanoribbons (g-i) are presented. The effect of electric field on the energy gap of selected GNR4 is shown in (j-m).

3.2 Doping and Electric field

In this subsection, we study the effect of edge and surface doping on the binding energy, energy gap, and total electric dipole moment (TEDM). The considered dopants are N, O, S, P atoms and

the O-B-O group similar to Ref. [27]. The dopants positions are shown in Fig. 3 (a-i) along with the values and direction of TEDM. The effect of electric field directed in x- and y- directions on the band gap of selected chiral nanoribbons are given in Fig. 3 (j-m).
The results show that the binding energy and the energy gap can be increased/decreased depending on the type and position of the dopant. From Table 1, all the considered cases show higher binding energy for edges doping than that for surface doping except for S and Cl doping. For instance, the O atom doped at the edges have two electrons that can form strong covalent bond with adjacent C-atoms, now the two C-atoms bound to O will have additional two electrons to form strong double bond with neighbor C atoms with dcc= 1.36 Å. This edge reconstruction will be found around all O-atoms which in turn will increase the binding energy [54,55]. These strong bonds passivate the localized edge electrons and form HOMO with extended pi-orbitals, see Fig. 3 g, that significantly widen the band gap to E_g=2.08 eV. The even larger band gap, E_g=2.66 eV, in O-B-O doped chiral GNRs is also explained by the passivation of edge states from C-atoms. The increase of the band gap by edge doping with O-B-O found here are in good agreement with experimental results in Ref. [27], namely Eg=3.33 eV. This difference in the energy gap could be a result of the higher number of O-B-O segments that widen the band gap and/or the approximation of the DFT calculation level. Therefore, our results not only agree with experimental results but also predict other means to tune the band structure such as type of dopant and its position.

If O-atoms are doped on the surface both the binding energy and band gap decrease. The broken bonds at the surface in this case, Fig. 3 d, will decrease the binding energy per atom for the nanoribbon and at the same time will create localized electrons around the broken bonds that strongly decrease the band gap to 0.07 eV. The case of edge doping with P-atoms, highest E_b=7.99 eV, is little different where the edge reconstruction result in double bond between P and C atoms and the effect on E_g is not high because each P atom has three outer electrons that interact with neighbour C-atoms. This explanation applies also for the doping with N, and B elements. The special case of S-doping, at the edges S atoms form single bonds with neighbor C-atoms that are weaker than C-O or C-C bonds, thus lower E_b. While the sulfur atoms on the surface will form three bonds with adjacent C-atoms, two covalent bonds and one coordinate covalent bond, thus and similar to edge doping by O-atoms, neighbour C-atoms will form C=C bonds, that enhance the binding energy.

The TEDM substantially affected by the doping, where the originally negligible (~2*10^-3 D) dipole moment in GNR4-W3-L4 could be increased to 28 (D) by surface doping with O-atoms or kept unchanged by edge doping with O-B-O. The values and direction of TEDM in N-, B-, and P-doped nanoribbons are comparable, ranging from 4 to 12 (D) as given in Table 1 and shown in Fig. 3. The TEDM strongly depends on the position of the dopants, for example doping OBO in the edge position shown in Fig. 3 e results in local dipoles from the upper edge in a direction opposite to that from the lower one thus cancel each other. While replacing the outer C-atoms at the edges (Fig. 3 c) result in a net TEDM=7.14 D. The electric field effect is another effective tool to tune the chiral GNR electronic properties, here we study the effect of electric field on three undoped nanoribbons with different widths (Fig. 3 j-l) and one doped with OBO (Fig. 3 m). An electric field applied in y-direction result in an oscillating band gap in undoped nanoribbons

and decreases the wide band gap in OBO doped ones. The x-directed electric field enlarges/narrows the band gap in GNRE4-W3-L4/the remaining selected nanoribbons, results in semiconductor to conductor transformation for other systems as seen in Fig. 3 (l). The peculiar behavior of the band gap under the electric field is mainly due to the nature of the low energy molecular orbitals whether they are edge states or bulk states and the direction of the field. For instance, y-directed field (parallel to the zigzag edge) will provide an oscillating effect on the low energy molecular orbitals at the zigzag edge. While the filed applied in x-direction (perpendicular to the zigzag edge) will increase the small E_g between the *edge states* in GNR4-W3-L4 and decrease the wide band gap between the *surface extended states* in doped GNR4-W3-L4-OBO similar to its effect on hexagonal flakes with zigzag edges reported in [56]. Similarly, the y-field in the latter case decreases the band gap. In contrast, x-directed field decreases the band gap in Fig. 3 (k, l), the decrease is simply due to the change in x-direction orientation with respect to width and length directions, this direction orientation is automatically adjusted by the Gaussian software. To avoid this confusion, it is convenient to relate the field direction to the GNR length such that electric field parallel to the length direction oscillates the band gap while that perpendicular to it enlarge it.

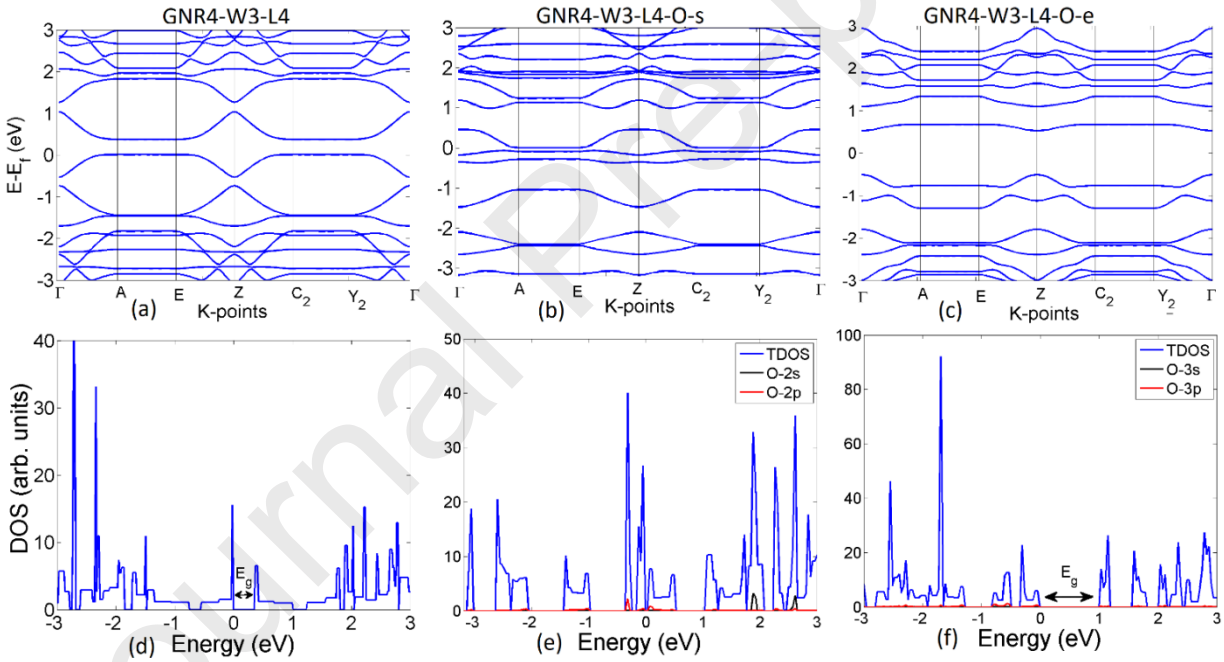

Fig. 4. Band structure and density of states for selected chiral GNR.

Here we provide additional calculations on periodic systems to generalize and confirm our results on finite nanoribbons, the selected periodic nanoribbons are GNR4-W3, GNR4-W3-O-s, GNR4-W3-O-e. The band structure, total density of states (TDOS), and dopant contribution to the TDOS for these systems are shown in Fig. (4). The band structure and TDOS of GNR4-W3-L4 show a band gap =0.35 eV, this value is lower than the obtained value in GNR4-W3-L9. This decrease is a result of the infinite length considered in periodic calculations, also the functional may affect the band gap. The tunable band structure by doping observed in finite systems occurs also in periodic nanoribbons where the band can be increased/decreased by doping with O atoms

at the edge/surface. Also the contribution of the dopant electrons to the low energy states is higher when these atoms doped at the surface than edge doping that confirms the previous conclusion on the origin of band structure changes after doping.

3.3 Optical properties

The optical properties of GNR4 are investigated using the TD-DFT calculations of the first 20 excited states. Fig. 5 presents the optical spectra of GNR4 under the effect of length (a), width (b), doping with different elements (c), and electric field (d). It is observed that increasing the length or width result in a noticeable red shift while in case of doping the absorption spectrum may have red shift or blue shift from the undoped GNR4-W3-L4 depending (Fig. 5 c) on the type and position of the dopant. The dominant absorption UV peak of GNR4-L1 at 273 (nm) can be smoothly red shifted to 2780 (nm) in GNR4-L9, similarly, increasing the width shifts the absorption maxima at 573 (nm) in GNR4-W1 to 2187 (nm) in GNR4-W6 (see the structure in Fig.1 l).

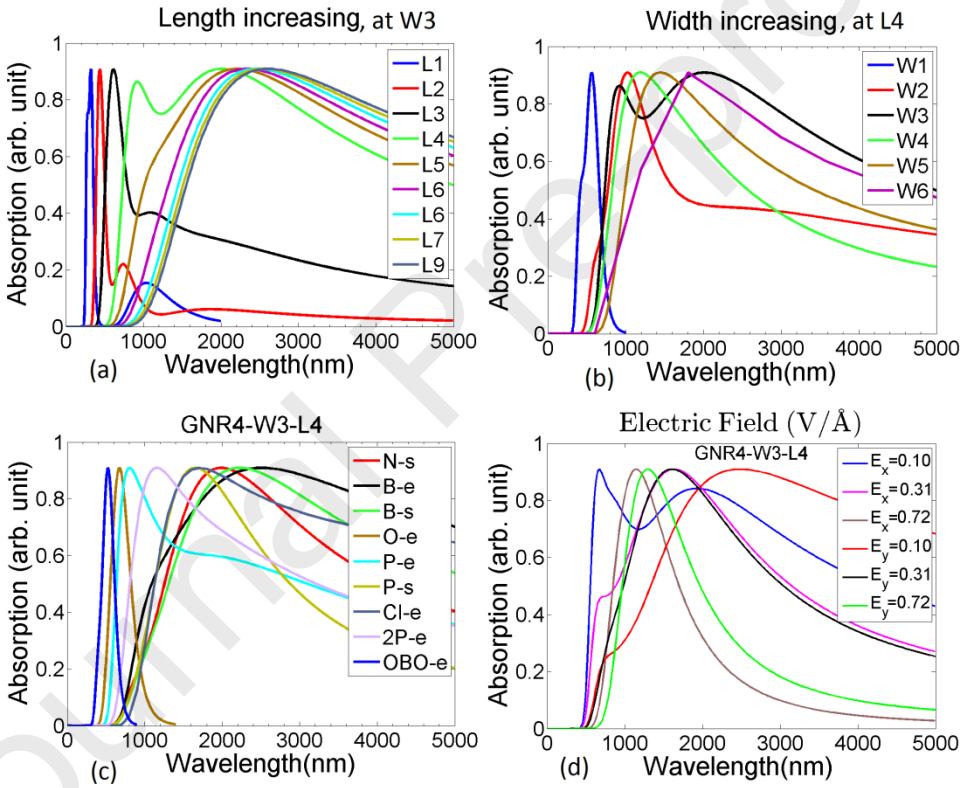

Fig. 5. Absorption spectra of GNR4 under the effect of length (a), width (b), doping (c), and in plane electric field.

It is observed that the absorption spectra as a function of length have a shoulder transition peak for small lengths, namely from L1 to L3, and disappear in higher lengths. The shoulder peak in L1 at 1037 (nm) is a result of transition from HOMO-LUMO with oscillator strength (f) equals 0.16. This transition becomes the dominant transition in higher lengths, L5-L9. The shoulders in L2 and L3 are mostly due to transitions from HOMO-1 to LUMO+1. Additionally, the absorption spectrum of a specific GNR4 can be tuned by doping, for example the two dominant transition peaks at 891 and 2453 (nm) in GNR4-W3-L4 exhibit blue shift to a single peak at 535 (nm) after doping with OBO at the edge (Fig. 5 c). While, doping with 2P atoms at the edge (the

structure in Fig. 2 e) shift these two peaks to a transition wavelength at 1165 nm or the significant red shifting to 3576 (nm) in case of doping with B at the edges. The optical spectra of GNR4-W3-L4 at selected electric field values (Fig. 5 d) show increase of the optical band gap by increasing the x-directed electric field, following the increase of the electronic band gap Fig. 3 (j), and oscillates as a function of the applied y-field.

The detailed information about the UV-Vis spectra of GNR subjected to the effect of length, width, and doping are given in Table 2, namely the oscillator strength, wavelength, excitation energy, dominant transition, and transition composition. The optical calculations for the remaining doped nanoribbons are given in Table S1 in supplementary material. It is noted from Table 2 that the two prominent transitions in L1 is a result of transitions from the ground state (S0) to the excited state S13 and to S20 with considerable high excitation energy 3.83 and 4.54 eV, respectively.

Table. 2. Optical parameters for the prominent excitations in selected chiral nanoribbons, f and λ are the excitation oscillator strength and wavelength. E_x, D_X, and TC are the excitation energy, dominant excitation, and transition composition, respectively.

Length						**Width**					
GNR -W3-	***f***	**λ (nm)**	**E_x (eV)**	**D_X**	**TC**	**GNR - L4-**	***f***	**λ (nm)**	**E_x (eV)**	**D_X**	**TC**
L1	0.43	324	3.83	S13	H-6→L 0.25 H-5→L 0.34 H-2→L+1 0.15 H-1→L+2 0.24 H→L+5 0.48	W1	1.34	573	2.16	S1	H→L 0.70
	0.62	273	4.54	S20	H-5→L -0.17 H-3→L+2 -0.12 H-2→L+1 0.49 H-2 →L+3 0.12 H-1→L+2 0.39 H →L+5 -0.19	W2	1.29	1034	1.19	S5	H-2→ L 0.45 H-1→ L+1 -0.19 H→ L 0.15 H→ L+2 0.49 L→H -0.13
L2	0.33	443	2.80	S17	H-4→L -0.21 H-3→L+1 -0.37 H-1→L+3 0.43 H-1→L+4 -0.13 H→L+5 -0.27 H→L+6 -0.11	W3	0.15	2453	0.51	S1	H-1→L 0.63 H→L+1 -0.30
							0.12	891	1.39	S12	H-3→L+1 0.12 H-2→L+2 0.57 H-1→L+1 0.10 H-1→L+3 -0.38
L3	0.20	667	1.86	S10	H-3→L+1 -0.22 H-2→L+2 0.66	W6	0.65	1494	0.83	S14	H-3→ H+1 0.29 H-3→ L+3 0.15 H-2→ L+2 0.47 H-1→ L+1 -0.22 H-1→ L+3 0.31 H→ L 0.28 H→ L+4 -0.13 L+1→ H-1 0.15 L→ H -0.24
L4	0.15	2453	0.51	S1	H-1 →L 0.63 H→L+1 -0.30						
	0.12	891	1.39	S12	H-3→L+1 0.12 H-2→L+2 0.57 H-1→L+1 0.10 H-1→L+3 -0.38						

L5	0.23	2576	0.48	S1	H →L 0.72 L → H -0.13	**Doping**					
L6	0.31	2658	0.47	S1	H → L 0.72 L → H -0.12	W3-N-e	0.15	2627	0.47	S1	H-L→ L 0.11 H→ L 0.71 L→ H -0.14
L7	0.39	2714	0.46	S1	H → L 0.72 L → H -0.10		0.16	637	1.95	S19	H-3 → L+3 0.66 H-2 → L+4 0.12
L8	0.46	2753	0.45	S1	H-1→ L+1 0.11 H → L 0.71	W3-OBO	3.05	535	2.32	S1	H-1 → L+1 -0.16 H → L 0.68
L9	0.54	2780	0.45	S1	H-1→L+1 -0.14 H → L 0.71	W3-P-s	2.30	1704	0.73	S1	H →L 0.70 L → H -0.14

These transitions composed of different transitions all of them are fare from the HOMO→LUMO (H→L) transition. For instance, the main transition in L1 from S0 to S13 is composed of transitions from H-6→L (12.5%), H-5 →L (23.5%), H-2→L+1 (4.4%), H-1 →L+2 (11.6%), and H →L+5 (45.2%). For L2 and L3 the dominant transitions are from S0 to S17 (2.80 eV) and from S0 to S10 (1.86), respectively. Which are also dominated by transitions far from H→L. Excitations contributed by transitions close to the H→L transition start to appear in L4 where the main excitations, S1, is contributed by H-1→L and H → L+1 with transition energy equals 0.51 eV. In Higher lengths starting from L5-L9, the dominant excitation is S0 →S1 which is contributed mainly by H→L transition with percent contribution >96%. In case of width, the contribution of H→L transition to the optical spectrum in small widths is more significant than that length case. The prominent excitation in W1, from S0 to S1 at λ= 573 (nm) is mainly due to H→ L (98.7%) transition. However, in larger widths, W4-W6, the main excitations are not mainly from H→L like in L5-L9 and contrarily other transitions participate in the excitation such as H-2→L+2 (44%) in W6. The transitions from higher orbitals to lower ones, like from L→H, represent a de-excitation that is neglected in our discussion. The contributions to the main excitations in doped nanoribbons depend on the type of dopant and its position. The main excitations in GNR4-W3-L4 doped with OBO and B (at the edge) are due to transitions from H to L while other transitions are involved in the main excitations when doped with Cl and P atoms at the edges (Table S1). It is worth noting that even though the main excitations in P edge doping occur at excitation energy, 1.71 eV, higher than the corresponding electronic band gap (0.55 eV), there is a considerable excitation at this low energies (see the shoulder peak in Fig. 5 for P-e). While the transition from H to L in Cl-doped case (Table S1) and due to the small energy gap, it will be involved in an excitation containing equal H→L excitation that have a small (4%) contribution to the optical spectrum.

4. Conclusion

In this work, the electronic and optical properties of chiral graphene nanoribbons are investigated using density functional theory calculations. The effects of length, width, doping, and electric field are taken into account. The optimized structures in addition to the positive frequencies from infrared spectra and positive binding energies confirm the stability of the considered systems.

The binding energy increases with increasing the width more than length increase due to the higher number of surface C-atoms, with three sigma bonds, in the former. Abrupt decrease in the band gap is observed when increasing width with respect to the smooth decrease as a function of length due to the lower number of the interactive edge states in the later. That decrease is a result of chirality which leads to the formation of strong edge bonds that in turn form molecular orbitals with energies deeper in the valance band than other edge bonds. The position of the dopant (edge or surface) is an important factor affecting the binding energy and the electronic properties. For instance, O-atoms at the edges have only two electrons for binding this will leave additional electrons in neighbor C-atoms that will form strong C=C bonds with other edge atoms that enhance the binding energy. In contrast, at the surface they will break some of the strong sigma bonds and therefore decrease the binding energy. The energy gap in the first case equals 2.08 eV because of the passivation of some of the edge electrons by the C=C bonds while in the second case the gap decreases to 0.07 eV due to the created localized energy states at the surface. The band gap can also be increased by OBO doping at the edges, which agree with the experimental results. The behavior of band structure for selected periodic nanoribbons under the effect of doping confirms and generalizes the results of the finite systems. The band gap oscillates under y-direction field in undoped nanoribbons and decreases in OBO doped ones. This peculiar behavior is a result of the different nature of the low energy states where they are localized edges states in the former and extended surface states in the later. Moreover, semiconductor to conductor transformation can be achieved by applying electric field in x-direction. The optical band gap increases/oscillates by applying x/y-electric field in a way similar to the behavior of the electronic band gap. The optical spectrum can be controlled by varying the length, the width, and by doping where a considerable red shift is observed by increasing width or length and by doping the absorption spectrum may experience red shift or blue shift depending on the dopant type and position.

Acknowledgement

This work is supported by National Natural Science Foundation of China (No. 11774178). HA acknowledges the postdoctoral funding by Talent Young Scientist Program (TYSP). VAS acknowledges support from the RCN CoE funding scheme (Grant No. 262633, ‘‘QuSpin’’). W. O. Younis (originally affiliated to Physics Department, Faculty of Science, Beni-Suef University, Beni-Suef City, Egypt) acknowledges the collaborative research between Beni-Suef University and IAU.

Supplementary Material

Further confirmation of stability is obtained from the positive frequencies in the infrared spectra for different chiral GNR before and after doping.

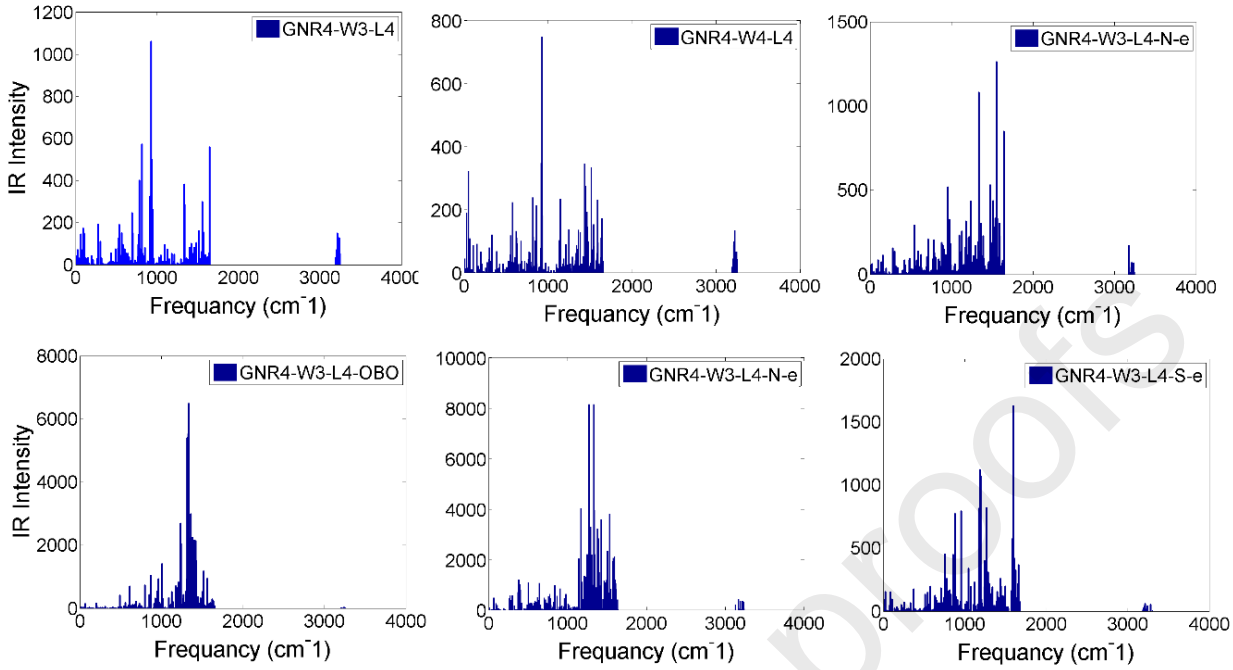

Fig. S1. Infrared spectra for selected chiral graphene nanoribbons before and after doping.

b- Optical parameters of doped nanoribbons

Table. S_1. The dominant excitations parameters in doped GNR-W3-L4 optical, f and λ are the excitation oscillator strength and wavelength. EX, DX, and TC are the excitation energy, dominant excitation, and transition composition, respectively.

Doping					
GNR4-W3-L4	***f***	**λ(nm)**	**E_x (eV)**	**DX**	**TC**
B-e	0.13	3576	0.35	S1	H → L 0.74 L → H -0.19
B-s	0.87	2565	0.48	S1	H-1 → L 0.19 H-1 → L+1 0.12 H → L 0.66 H → L+1 0.25 L→H -0.25
CL-e	0.18	1446	0.86	S17	H-3→ L+2 0.15 H-2→ L+2 0.48 H-1→ L+1 0.13 H-1→ L+2 0.11 H-1→L+3 0.44 H→ L -0.14 L→ H 0.13
N-s	1.41	2151	0.58	S1	H-2 →L -0.17 H-2 →L+1 0.10 H-1 → L 0.69 H-1 → L+1 0.14 L→ H -0.23

O-e	2.55	692	1.79	S1	H-2 → L+1 0.14 H → L 0.68
O-s	0.07	4069	0.31	S6	H-3 → L 0.61 H → L 0.21 H → L+1 0.28 L → H -0.14
2P-e	0.08	1165	1.06	S12	H → L 0.73 L → H -0.15
P-e	0.15	725	1.71	S20	H-4 → L+1 0.11 H-4 →L+2 0.14 H-3 → L+3 0.62 H-1 → L+4 -0.11

REFERANCES

[1] M. Terrones, A. R. Botello-Méndez, J. Campos-Delgado, F. López-Urías, Y. I. Vega-Cantú, F. J. Rodríguez-Macías, A. L. Elías, E. Muñoz-Sandoval, A. G. Cano-Márquez, and J.-C. Charlier, Graphene and graphite nanoribbons: Morphology, properties, synthesis, defects and applications. Nano Today **5**, 351 (2010).

[2] O. V. Yazyev, A Guide to the Design of Electronic Properties of Graphene Nanoribbons. Acc. Chem. Res. **46**, 2319 (2013).

[3] V. Meunier, A. G. Souza Filho, E. B. Barros, and M. S. Dresselhaus, Physical properties of low-dimensional sp2-based carbon nanostructures. Rev. Mod. Phys. **88**, 025005 (2016).

[4] H.-C. Chung, C.-P. Chang, C.-Y. Lin, and M.-F. Lin, Electronic and optical properties of graphene nanoribbons in external fields. Phys. Chem. Chem. Phys. **18**, 7573 (2016).

[5] A. Celis, M. N. Nair, A. Taleb-Ibrahimi, E. H. Conrad, C. Berger, W. A. de Heer, and A. Tejeda, Graphene nanoribbons: fabrication, properties and devices. J. Phys. D. Appl. Phys. **49**, 143001 (2016).

[6] Y. Yano, N. Mitoma, H. Ito, and K. Itami, A Quest for Structurally Uniform Graphene Nanoribbons: Synthesis, Properties, and Applications. J. Org. Chem. **85**, 4 (2020).

[7] J. Cai, P. Ruffieux, R. Jaafar, M. Bieri, T. Braun, S. Blankenburg, M. Muoth, A. P. Seitsonen, M. Saleh, X. Feng, K. Müllen, and R. Fasel, Atomically precise bottom-up fabrication of graphene nanoribbons. Nature **466**, 470 (2010).

[8] A. Narita, X. Feng, Y. Hernandez, S. A. Jensen, M. Bonn, H. Yang, I. A. Verzhbitskiy, C. Casiraghi, M. R. Hansen, A. H. R. Koch, G. Fytas, O. Ivasenko, B. Li, K. S. Mali, T. Balandina, S. Mahesh, S. De Feyter, and K. Müllen, Synthesis of structurally well-defined and liquid-phase-processable graphene nanoribbons. Nat. Chem. **6**, 126 (2014).

[9] T. H. Vo, M. Shekhirev, D. A. Kunkel, M. D. Morton, E. Berglund, L. Kong, P. M. Wilson, P. A. Dowben, A. Enders, and A. Sinitskii, Large-scale solution synthesis of narrow graphene nanoribbons. Nat. Commun. **5**, 3189 (2014).

[10] H. Huang, D. Wei, J. Sun, S. L. Wong, Y. P. Feng, A. H. C. Neto, and A. T. S. Wee, Spatially resolved electronic structures of atomically precise armchair graphene nanoribbons. Sci. Rep. **2**, 1 (2012).

[11] C. Ma, L. Liang, Z. Xiao, A. A. Puretzky, K. Hong, W. Lu, V. Meunier, J. Bernholc, and A.-P. Li, Seamless Staircase Electrical Contact to Semiconducting Graphene Nanoribbons. Nano Lett. **17**, 6241 (2017).

[12] O. Deniz, C. Sánchez-Sánchez, T. Dumslaff, X. Feng, A. Narita, K. Müllen, N. Kharche, V. Meunier, R. Fasel, and P. Ruffieux, Revealing the Electronic Structure of Silicon Intercalated Armchair Graphene

Nanoribbons by Scanning Tunneling Spectroscopy. Nano Lett. **17**, 2197 (2017).

[13] S. Wang, N. Kharche, E. Costa Girão, X. Feng, K. Müllen, V. Meunier, R. Fasel, and P. Ruffieux, Quantum Dots in Graphene Nanoribbons. Nano Lett. **17**, 4277 (2017).

[14] Z. Chen, H. I. Wang, N. Bilbao, J. Teyssandier, T. Prechtl, N. Cavani, A. Tries, R. Biagi, V. De Renzi, X. Feng, M. Kläui, S. De Feyter, M. Bonn, A. Narita, and K. Müllen, Lateral Fusion of Chemical Vapor Deposited N = 5 Armchair Graphene Nanoribbons.. J. Am. Chem. Soc. **139**, 9483 (2017).

[15] P. Ruffieux, S. Wang, B. Yang, C. Sánchez-Sánchez, J. Liu, T. Dienel, L. Talirz, P. Shinde, C. A. Pignedoli, D. Passerone, T. Dumslaff, X. Feng, K. Müllen, and R. Fasel, On-surface synthesis of graphene nanoribbons with zigzag edge topology. Nature **531**, 489 (2016).

[16] P. H. Jacobse, K. A. Simonov, M. J. J. Mangnus, G. I. Svirskiy, A. V Generalov, A. S. Vinogradov, A. Sandell, N. Mårtensson, A. B. Preobrajenski, and I. Swart, One Precursor but Two Types of Graphene Nanoribbons: On-Surface Transformations of 10,10′-Dichloro-9,9′-bianthryl on Ag(111). J. Phys. Chem. C acs. jpcc.8b12209 (2019).

[17] V. A. Saroka and K. G. Batrakov, Zigzag-Shaped Superlattices on the Basis of Graphene Nanoribbons: Structure and Electronic Properties. Russ. Phys. J. **59**, 633 (2016).

[18] V. A. Saroka, K. G. Batrakov, V. A. Demin, and L. A. Chernozatonskii, Band gaps in jagged and straight graphene nanoribbons tunable by an external electric field. J. Phys. Condens. Matter **27**, 145305 (2015).

[19] V. A. Saroka, K. G. Batrakov, and L. A. Chernozatonskii, Edge-modified zigzag-shaped graphene nanoribbons: Structure and electronic properties. Phys. Solid State **56**, 2135 (2014).

[20] M. Mehdi Pour, A. Lashkov, A. Radocea, X. Liu, T. Sun, A. Lipatov, R. A. Korlacki, M. Shekhirev, N. R. Aluru, J. W. Lyding, V. Sysoev, and A. Sinitskii, Laterally extended atomically precise graphene nanoribbons with improved electrical conductivity for efficient gas sensing. Nat. Commun. **8**, 820 (2017).

[21] P. S. Costa, J. D. Teeter, A. Enders, and A. Sinitskii, Chevron-based graphene nanoribbon heterojunctions: Localized effects of lateral extension and structural defects on electronic properties. Carbon N. Y. **134**, 310 (2018).

[22] J. D. Teeter, P. Zahl, M. Mehdi Pour, P. S. Costa, A. Enders, and A. Sinitskii, On-Surface Synthesis and Spectroscopic Characterization of Laterally Extended Chevron Graphene Nanoribbons. ChemPhysChem **20**, 2281 (2019).

[23] M. Di Giovannantonio, K. Eimre, A. V. Yakutovich, Q. Chen, S. Mishra, J. I. Urgel, C. A. Pignedoli, P. Ruffieux, K. Müllen, A. Narita, and R. Fasel, On-Surface Synthesis of Antiaromatic and Open-Shell Indeno[2,1b]fluorene Polymers and Their Lateral Fusion into Porous Ribbons. J. Am. Chem. Soc. **141**, 12346 (2019).

[24] J. Liu, B.-W. Li, Y.-Z. Tan, A. Giannakopoulos, C. Sanchez-Sanchez, D. Beljonne, P. Ruffieux, R. Fasel, X. Feng, and K. Müllen, Toward Cove-Edged Low Band Gap Graphene Nanoribbons. J. Am. Chem. Soc. **137**, 6097 (2015).

[25] D. Beyer, S. Wang, C. A. Pignedoli, J. Melidonie, B. Yuan, C. Li, J. Wilhelm, P. Ruffieux, R. Berger, K. Müllen, R. Fasel, and X. Feng, Correction to "Graphene Nanoribbons Derived from Zigzag Edge-Encased Poly(para-2,9-dibenzo[bc, kl]coronenylene) Polymer Chains". J. Am. Chem. Soc. **141**, 2843 (2019).

[26] P. Han, K. Akagi, F. Federici Canova, H. Mutoh, S. Shiraki, K. Iwaya, P. S. Weiss, N. Asao, and T. Hitosugi, Bottom-up graphene-nanoribbon fabrication reveals chiral edges and enantioselectivity. ACS Nano **8**, 9181 (2014).

[27] X.-Y. Wang, J. I. Urgel, G. B. Barin, K. Eimre, M. Di Giovannantonio, A. Milani, M. Tommasini, C. A. Pignedoli, P. Ruffieux, X. Feng, R. Fasel, K. Müllen, and A. Narita, Bottom-Up Synthesis of Heteroatom-Doped Chiral Graphene Nanoribbons. J. Am. Chem. Soc. **140**, 9104 (2018).

[28] N. Merino-Díez, J. Li, A. Garcia-Lekue, G. Vasseur, M. Vilas-Varela, E. Carbonell-Sanromà, M. Corso, J.

E. Ortega, D. Peña, J. I. Pascual, and D. G. de Oteyza, Unraveling the Electronic Structure of Narrow Atomically Precise Chiral Graphene Nanoribbons. J. Phys. Chem. Lett. **9**, 25 (2018).

[29] D. G. de Oteyza, A. García-Lekue, M. Vilas-Varela, N. Merino-Díez, E. Carbonell-Sanromà, M. Corso, G. Vasseur, C. Rogero, E. Guitián, J. I. Pascual, J. E. Ortega, Y. Wakayama, and D. Peña, Substrate-Independent Growth of Atomically Precise Chiral Graphene Nanoribbons. ACS Nano **10**, 9000 (2016).

[30] F. Schulz, P. H. Jacobse, F. F. Canova, J. van der Lit, D. Z. Gao, A. van den Hoogenband, P. Han, R. J. M. Klein Gebbink, M.-E. Moret, P. M. Joensuu, I. Swart, and P. Liljeroth, Precursor Geometry Determines the Growth Mechanism in Graphene Nanoribbons. J. Phys. Chem. C **121**, 2896 (2017).

[31] V. A. Saroka, M. V. Shuba, and M. E. Portnoi, Optical selection rules of zigzag graphene nanoribbons. Phys. Rev. B **95**, 155438 (2017).

[32] V. A. Saroka, A. L. Pushkarchuk, S. A. Kuten, and M. E. Portnoi, Hidden correlation between absorption peaks in achiral carbon nanotubes and nanoribbons. J. Saudi Chem. Soc. **22**, 985 (2018).

[33] R. B. Payod and V. A. Saroka, Ab initio study of absorption resonance correlations between nanotubes and nanoribbons of graphene and hexagonal boron nitride. Semiconductors **53**, 1929 (2019).

[34] R. B. Payod, D. Grassano, G. N. C. Santos, D. I. Levshov, O. Pulci, and V. A. Saroka, 2N+4-rule and an atlas of bulk optical resonances of zigzag graphene nanoribbons. Nat. Commun. **11**, 82 (2020).

[35] M. Berahman, M. Asad, M. Sanaee, and M. H. Sheikhi, Optical properties of chiral graphene nanoribbons: a first principle study. Opt. Quantum Electron. **47**, 3289 (2015).

[36] Y. Lu, W.-G. Lu, and L. Wang, Structure Dependence of Excitonic Effects in Chiral Graphene Nanoribbons. Chinese Phys. Lett. **34**, 017102 (2017).

[37] J. Overbeck, G. B. Barin, C. Daniels, M. L. Perrin, O. Braun, Q. Sun, R. Darawish, M. De Luca, X.-Y. Wang, T. Dumslaff, A. Narita, K. Müllen, P. Ruffieux, V. Meunier, R. Fasel, and M. Calame, A Universal Length-Dependent Vibrational Mode in Graphene Nanoribbons. ACS Nano **13**, 13083 (2019).

[38] V. A. Saroka, H. Abdelsalam, V. A. Demin, D. Grassano, S. A. Kuten, A. L. Pushkarchuk, and O. Pulci, Absorption in Finite-Length Chevron-Type Graphene Nanoribbons. Semiconductors **52**, 1890 (2018).

[39] S. Kawai, S. Saito, S. Osumi, S. Yamaguchi, A. S. Foster, P. Spijker, and E. Meyer, Atomically controlled substitutional boron-doping of graphene nanoribbons. Nat. Commun. **6**, 6 (2015).

[40] J.-C. Blancon, M. Paillet, H. N. Tran, X. T. Than, S. A. Guebrou, A. Ayari, A. S. Miguel, N.-M. Phan, A.-A. Zahab, J.-L. Sauvajol, N. D. Fatti, and F. Vallée, Direct measurement of the absolute absorption spectrum of individual semiconducting single-wall carbon nanotubes. Nat. Commun. **4**, (2013).

[41] F. Yao, C. Liu, C. Chen, S. Zhang, Q. Zhao, F. Xiao, M. Wu, J. Li, P. Gao, J. Zhao, X. Bai, S. Maruyama, D. Yu, E. Wang, Z. Sun, J. Zhang, F. Wang, and K. Liu, Measurement of complex optical susceptibility for individual carbon nanotubes by elliptically polarized light excitation. Nat. Commun. **9**, 3387 (2018).

[42] M.J. Frisch, G.W. Trucks, H.B. Schlegel, G.E. Scuseria, et al., Gaussian 16, Revision B.01, Gaussian, Inc., Wallingford, CT, 2016.

[43] A. D. Becke, A new mixing of Hartree–Fock and local density-functional theories. J. Chem. Phys. 98, 5648 (1993).

[44] C. Lee, W. Yang, P.G. Parr, Development of the Colle-Salvetti correlation-energy formula into a functional of the electron density. Phys. Rev. B 37,785 (1998).

[45] K. D. Dobbs and W. J. Hehre, Molecular orbital theory of the properties of inorganic and organometallic compounds 5. Extended basis sets for first-row transition metals. J. Comput. Chem. 8, 880 (1987).

[46] H. Abdelsalam, H. Elhaes, M. A. Ibrahim, Tuning electronic properties in graphene quantum dots by chemical functionalization: Density functional theory calculations. Chem. Phys. Lett., 696, 138 (2018).

[47] H. Zheng and W. Duley, First-principles study of edge chemical modifications in graphene nanodots. Phys. Rev B 78, 045421 (2008).

[48] H. Abdelsalam, V.A. Saroka, W.O. Younis, Edge functionalization of finite graphene nanoribbon superlattices. Superlattice Microst. 129, 54 (2019).

[49] G. Kresse, J. Hafner, Ab initio molecular dynamics for liquid metals, Phys. Rev. B 47, 558 (1993).

[50] P. E. Blöchl, Projector augmented-wave method. Phys. Rev. B 50, 17953 (1994).

[51] G. Kresse, J. Furthmuller, Efficiency of ab-initio total energy calculations for metals and semiconductors using a plane-wave basis set. Comput Mater Sci. 6, 15 (1996).

[52] G. Kresse, Furthmuller, Efficient iterative schemes for ab initio total-energy calculations using a plane-wave basis set. Phys. Rev. B 54, 11169 (1996).

[53] J. P. Perdew, K. Burke, M. Ernzerhof, Generalized Gradient Approximation Made Simple. Phys. Rev. Lett. 77, 3865 (1996).

[54] F. Ersan, O. Ü. Aktürk, E. Aktürk, S. Ciraci, Metal–Insulator transition and heterostructure formation by glycines self-assembled on defect-patterned graphene. J. Phys. Chem. C 122, 14598 (2018).

[55] H. Abdelsalam, W. O. Younis, V. A. Saroka, N. H. Teleb, S. Yunoki, Q. Zhang, Interaction of hydrated metals with chemically modified hexagonal boron nitride quantum dots: wastewater treatment and water splitting. Phys. Chem. Chem. Phys, 22, 566 (2020).

[56] H. Abdelsalam, V. A. Saroka, I. Lukyanchuk, and M. E. Portnoi, Multilayer phosphorene quantum dots in an electric field: Energy levels and optical absorption. J. Appl. Phys. 124, 124303 (2018).

Credit Author Statement

H. Abdelsalam, V.A. Saroka, built the structures and the computational framework. M.M. Atta performed the optical calculations. H. Abdelsalam analyzed the data and wrote the manuscript with support from V.A. Saroka and M.M. Atta. W.O. Younis performed the density functional theory calculations and discussion of the results. Q. Zhang provided discussion, comments and supervision on the research project.